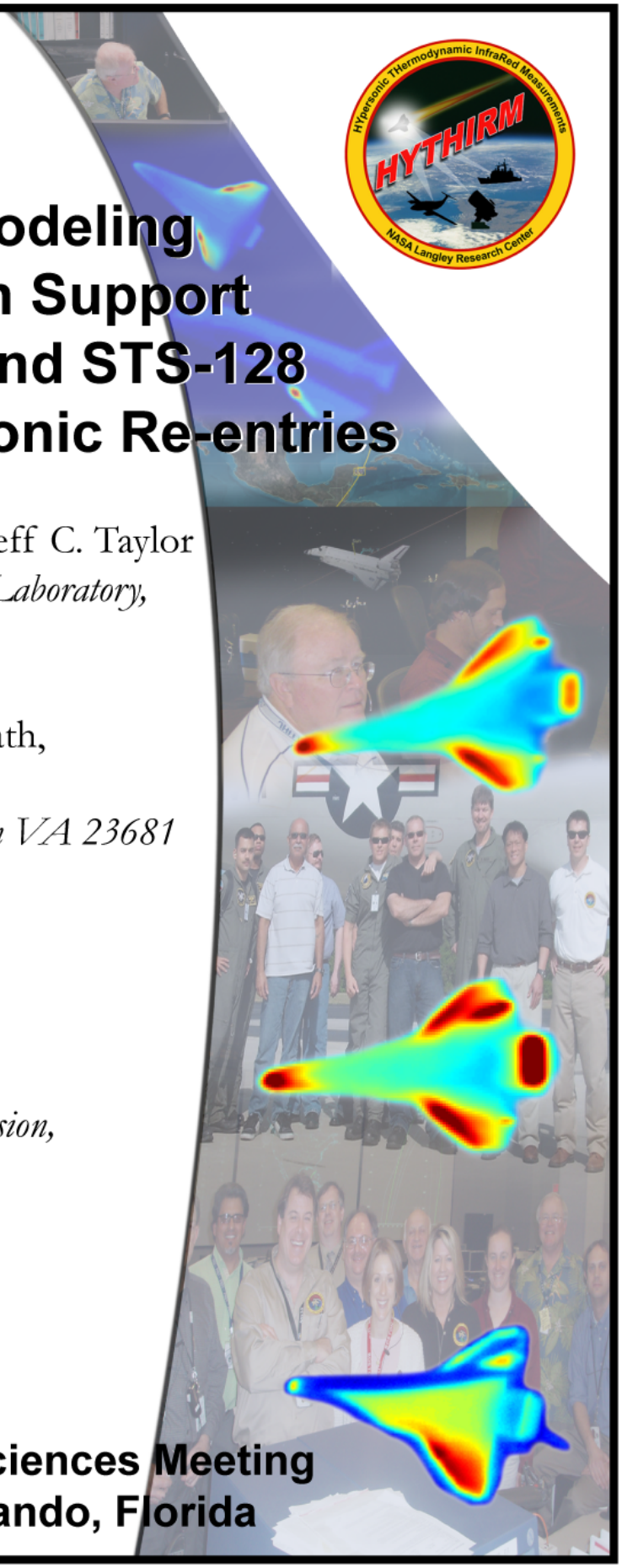

AIAA-2010-245
HYTHIRM Radiance Modeling and Image Analyses in Support of STS-119, STS-125 and STS-128 Space Shuttle Hypersonic Re-entries

David M. Gibson, Thomas S. Spisz , Jeff C. Taylor
Johns Hopkins University Applied Physics Laboratory, Laurel, MD 20723

Joseph N. Zalameda, Thomas J. Horvath, Deborah M. Tomek
NASA Langley Research Center, Hampton VA 23681

Alan B. Tietjen
ISTEF-CSC, KSC, FL 32899

Steve Tack
Naval Air Warfare Center - Weapons Division, Pt. Mugu, CA 93042

Brett C. Bush
Raytheon/Photon Research Associates, San Diego, CA 92121

48th AIAA Aerospace Sciences Meeting
January 4-7 2010, Orlando, Florida

45th AIAA Aerospace Sciences Meeting AIAA 2010-245
Jan. 4-7, 2010, Orlando, FL

HYTHIRM Radiance Modeling and Image Analyses in Support of STS-119, STS-125 and STS-128 Space Shuttle Hypersonic Re-entries

David M. Gibson, Thomas S. Spisz and Jeff C. Taylor
The Johns Hopkins University Applied Physics Laboratory, Laurel, MD 20723

Joseph N. Zalameda, Thomas J. Horvath and Deborah M. Tomek
NASA Langley Research Center, Hampton VA 23681

Alan B. Tietjen
ISTEF-CSC, Kennedy Space Center, FL 32899

Steve Tack
Naval Air Warfare Center - Weapons Division, Pt. Mugu, CA 93042

Brett C. Bush
Raytheon/Photon Research Associates, San Diego, CA 92121

We provide the first geometrically accurate (i.e., 3-D) temperature maps of the entire windward surface of the Space Shuttle during hypersonic reentry. To accomplish this task we began with estimated surface temperatures derived from CFD models at integral high Mach numbers and used them, the Shuttle's surface properties and reasonable estimates of the sensor-to-target geometry to predict the emitted spectral radiance from the surface (in units of W sr^{-1} m^{-2} nm^{-1}). These data were converted to sensor counts using properties of the sensor (e.g. aperture, spectral band, and various efficiencies), the expected background, and the atmosphere transmission to inform the optimal settings for the near-infrared and mid-wave IR cameras on the Cast Glance aircraft. Once these data were collected, calibrated, edited, registered and co-added we formed both 2-D maps of the scene in the above units and 3-D maps of the bottom surface in temperature that could be compared with not only the initial inputs but also thermocouple data from the Shuttle itself. The 3-D temperature mapping process was based on the initial radiance modeling process. Here temperatures were "guessed" for each node in a well-resolved 3-D framework, a radiance model was produced and compared to the processed imagery, and corrections to the temperature were estimated until the iterative process converged. This process did very well in characterizing the temperature structure of the large asymmetric boundary layer transition the covered much of the starboard bottom surface of STS-119 Discovery. Both internally estimated accuracies and differences with CFD models and thermocouple measurements are at most a few percent. The technique did less well characterizing the temperature structure of the turbulent wedge behind the trip due to limitations in understanding the true sensor resolution. (Note: Those less inclined to read the entire paper are encouraged to read an Executive Summary provided at the end.)

Acronyms

ABLT = Asymmetric Boundary Layer Transition
BLT = Boundary Layer Transition
BRDF = Bi-directional reflectance distribution function
CFD = Computational Fluid Dynamics
CG = Cast Glance
DTO = Detailed Test Objective
ISAFE = Infrared Sensing Aeroheating Flight Experiment

MWIR = Mid-wave Infrared
NIR = Near Infrared
PCA = Point of Closest Approach
PSF = Point Spread Function
RCC = Reinforced Carbon-Carbon
RCG = Reaction Cured Glass
STK = Satellite Took Kit
TC = Thermocouple
TPS = Thermal Protection System
TSP = Test Support Position

I. Introduction

High resolution calibrated infrared imagery of the Space Shuttle was obtained during hypervelocity atmospheric entry's of the STS-119, STS-125 and STS-128 missions and has provided information on the distribution of surface temperature and the state of the airflow over the windward surface of the Orbiter during descent. On Space Shuttle Discovery's STS-119 and STS-128 missions, NASA flew a specially modified tile and instrumentation package to monitor heating effects from boundary layer transition during re-entry. Boundary layer transition occurs when the smooth, laminar flow of air close to the Shuttle's surface is disturbed and becomes turbulent – resulting in temperature increases. On STS-119, the airflow on the port wing was deliberately disrupted by a four-inch wide and quarter-inch tall "speed bump." Built into a modified tile this "trip" was intended to promote transition to turbulence near Mach 15. In coordination with this flight experiment, a US Navy NP-3D Orion aircraft was flown 26 nautical miles below Discovery and remotely monitored surface temperature of the Orbiter at Mach 8.4 using a long-range infrared optical package referred to as Cast Glance. The thermal imagery complemented temperature data collected with an onboard instrumentation package consisting of 10 surface thermocouples. Approximately two months later, the same Navy aircraft successfully monitored the surface temperatures of STS-125 Atlantis traveling at approximately Mach 14.3 during its return from a successful Hubble repair mission. The STS-128 Discovery mission followed in September 2009 at approximately Mach 14.7, but this time the "trip" was taller, 0.35 in, intended to promote transition to turbulence at about Mach 18.

Collectively, the spatially resolved global thermal measurements made during these hypersonic re-entries were intended to provide critical flight data intended to reduce the uncertainty associated with present day ground-to-flight extrapolation techniques and current state-of-the-art empirical boundary-layer transition or turbulent heating prediction methods. Laminar and turbulent flight data are considered critical for the validation of physics-based, semi-empirical boundary-layer transition prediction methods. These data also stimulate the validation of laminar numerical chemistry models and the development of turbulence models supporting NASA's next-generation spacecraft under the Constellation program. The motivations behind what is now known as the Hypersonic Thermal Infrared Measurements (HYTHIRM) Project, as well as descriptions of its key aspects, are detailed in Ref. 7 and 8. We also refer the reader to Refs. 5 and 6 for relevant information on the NIR imaging system used onboard a Navy Cast Glance aircraft, the raw intensity imagery collected, as well as its calibration.

In this paper, we first describe in detail a radiance model that was used to estimate the Shuttle spectral irradiance at the focal plane array during re-entry and how the output from this model was used pre-flight to optimize the integration time of both the NIR and the MWIR sensors aboard the aircraft. This enabled exploitation of each sensor's full dynamic range while mitigating saturation.

Next we describe the data reduction processes. Since the processing of the thermal imagery was made difficult because all three re-entries were observed in full daylight we spend a significant amount of effort describing how we correct for atmospheric scattering into the scenes. Later we describe several techniques used to correct the data on an image-by-image basis that assure accurate Shuttle surface irradiances have been determined (including the proper emissivity values) so that accurate surface temperatures can be calculated. In particular, we show how we applied rigorous analytical image registration methods post-flight as well as flight orientation information from both the Shuttle and the Cast Glance aircraft to remove the geometric effects of non-orthogonal projection onto the image plane. Next, we describe how we determined temperatures locally and mapped them, first in 2-D and later in 3-D to the actual Shuttle geometry. These radiometrically-determined thermographs provide temperature information at

specific locations that can be compared to those measured by the Shuttles' surface thermocouples. In doing so, we provide particular insight into the uncertainty analysis and the accuracy of our methods.

In the last section of this paper we present analyses highlights from all three missions. As anticipated, the imagery from STS-125 shows smooth spatial and temporal variations across the bottom surface indicative of laminar flow. Only on Atlantis' nose, its wing leading edges, and in the regions of the aileron and aft ramp splits, shock effects drive the temperatures significantly higher. We also see evidence of a wake and a condensation trail behind a Shuttle. Since an Orbiter's surface is not ablative, neither result was expected. Next we present the STS-128 imagery and results. Both are well in family with the predictions and the STS-128 imagery. This was also expected since the velocities of the two shuttles were so similar at the time of observation. Finally, we present the data for STS-119 and its interpretation. This mission provided the most complex, visually interesting results, not only because Shuttle Discovery carried a small "trip" on the lower, windward surface of its port wing but because it exhibited a significant asymmetric boundary layer transition (ABLT).

For this paper we have also taken the extra step to provide an Executive Summary at the end. That information plus that gleaned from the figures and tables provide a quick way to view this entire work.

II. Radiance Modeling

In this section, we describe the various components used to take NASA-provided computational fluid dynamics (CFD) solutions of the Orbiters' surface temperature distributions to generate simulated radiance maps in both the near infrared (NIR) and mid-wave infrared (MWIR) bands. These estimates were then combined with calibration data to estimate the focal plane array (FPA) pixel responses in sensor counts. For the NIR sensor pixel map predictions, a series of maps were generated to span the possible sensor integration times so that the Cast Glance crew might use them to help choose optimal integration times to avoid saturation yet take full advantage of the sensor dynamic range capabilities. The overall schema is presented in Fig. 1. Because of the complexity with MWIR focal plane nonuniformity corrections, in-band radiance maps were provided to the Cast Glance team to feed through their MWIR sensor model to aid integration time settings.

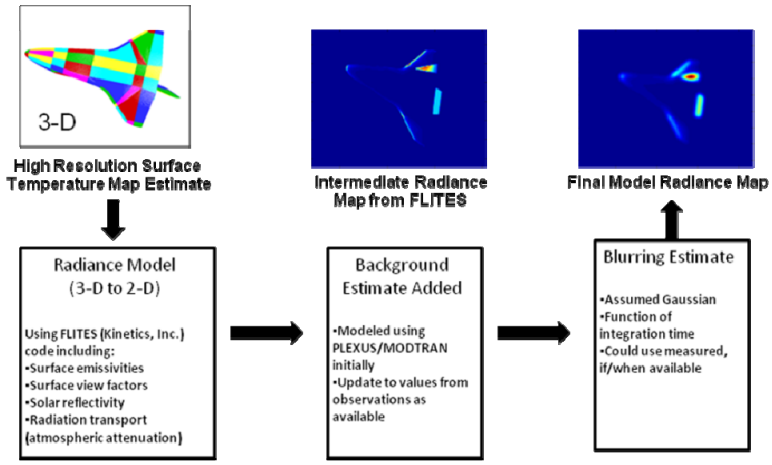

Figure 1. Schema for the production of radiance maps from NASA-supplied temperature maps.

A. Input Temperature Maps

Preflight calculations of the Shuttle flying at nominally 40° angle of attack with no sideslip were performed at a series of freestream Mach numbers. Both fully laminar and turbulent boundary layers were used as inputs for the radiance modeling. Wood ***et al***.[8] describe the CFD methodology used for our subsequent calculations in more detail.

We note here that the CFD geometry does not include the body flap, elevon gaps or the engine section in the aft region. The body flap, however, is a significant contributor to the thermal signatures. Therefore, we added an

estimate of the body flap geometry and set it to a uniform temperature based on prior missions for nominal body flap angles as a function of freestream Mach number. Furthermore, in keeping with the approaches also used by the CFD modelers, without ***a priori*** knowledge of the control surface angles, all control surfaces (ailerons, flaps, rudder, and body flap) were set to the neutral position (***i.e.***, zero degrees relative to the structure to which they are attached.)

The computational grid was converted to a finite element format for use in the radiance modeling code. Each computational surface mesh consists of 213,246 vertices grouped into 203,586 quadrilateral surface facets.

The described CFD thermal maps provided input bases for all cases where the Orbiters were expected to be fully laminar (***e.g.,*** for higher Mach numbers) or fully turbulent (***e.g.***, for lower Mach numbers). Radiation equilibrium conditions were assumed. To account for the BLT DTO wedge experiment flown on Discovery during STS-119 and STS-128, the following "modifications" were performed. Based on previous flight experience and wind tunnel tests[11] an expected "wedge" region was identified on the appropriate part of the windward side of the port wing. Outside of this "wedge," surface temperatures corresponding to a fully-developed laminar flow were assumed. Inside this "wedge," fully turbulent surface temperatures were assumed. Despite the obvious approximations of such an approach, this is ideal for providing preflight predictions where the goal is to allow for an appropriately sized region of higher temperatures. If needed these adjusted radiance modeling predictions would allow the Cast Glance crew to alter the NIR sensor integration times. An example of the CFD grid (without body flap) and the input temperature distribution including a turbulent wedge region for Mach 15 is shown below in Fig. 2.

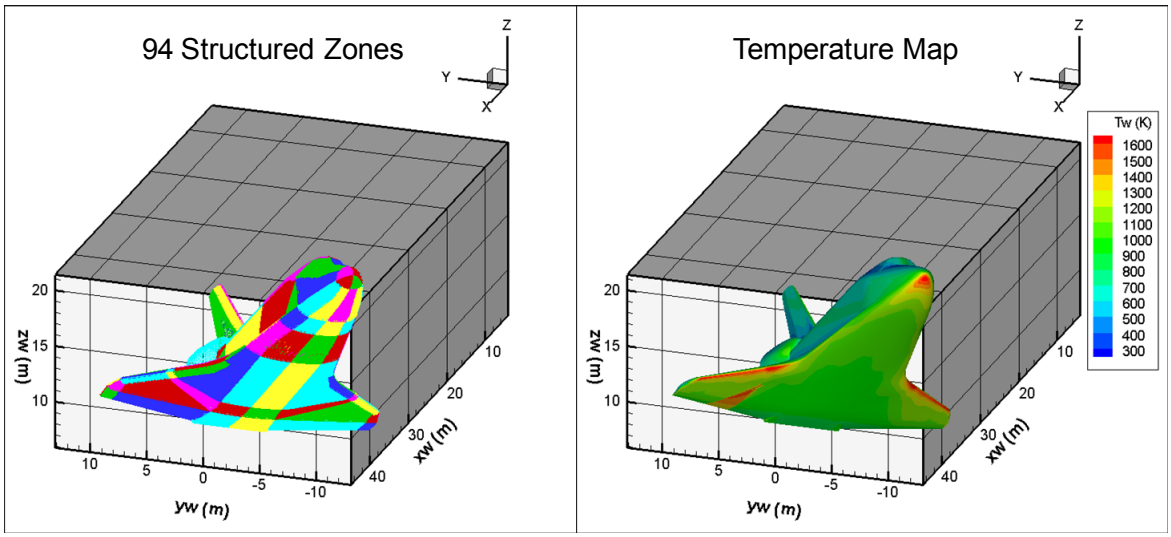

Figure 2. CFD temperature mesh (left) and input temperature map (right). The temperatures and wedge opening angle are characteristic of a Mach 15 flow**.**

B. Optical System Characterization

The Cast Glance NIR and MWIR optical systems have been described by Zalameda ***et al.***[6] Both are based on relatively long focal length Cassegrain telescopes designed to allow the image point spread function (PSF) to be oversampled. However, with so many optical components such as steering mirrors, windows, beam splitters and filters, the instrumental PSF is assuredly far from theoretical.

Though the radiance model is capable of integrating over arbitrary spectral response functions, the true spectral responses of the NIR and MWIR sensors have not been completely characterized. Therefore, the spectral responses for the NIR and the MWIR sensors were chosen to agree with those from the calibration reductions, ***i.e.***, square "top hat" responses. The NIR and MWIR sensor ranges used were 0.843-1.1 microns and 3.4-4.9 microns (with a CO_2 notch filter), respectively.

It is the apparent PSF of a functional optical system that significantly impacts the achievable spatial resolution and, ultimately, the radiometric errors in regions of sharp spatial gradients. In the cases of the Cast Glance sensor, the purely optical point spread function is "widened" by atmospheric turbulence, aircraft induced turbulence, tracking stability, jitter, and vibrations. All contribute in not necessarily constant or symmetric ways to the apparent

point spread functions at any time. Though not rigorously measured for the three missions for various good reasons, the apparent point spread function for the NIR imagery appears to be about 3.5 pixels in diameter. For the radiance modeling, the shape is assumed a symmetric Gaussian which appears to be a reasonable approximation based on the imagery analysis to date.

C. FLITES

The radiance modeling "engine" used for the radiance model is the Fast Line-of-sight Imagery for Target and Exhaust Signatures (FLITES) code.[1] FLITES is a robust DoD scene generation program capable of producing high fidelity signatures for infrared applications. Both the availability of this new tool -- which takes advantage of many modern computational acceleration techniques, accounting for a range of both emissive and reflective contributions to the signatures -- and having a validation and verification traceability across a wide range of problems made it attractive for use for Shuttle radiance modeling.

D. Surface Optical Properties

A major source of uncertainty in the radiance modeling resides in the optical properties of the Orbiter TPS surfaces. The windward side of the orbiter is covered predominantly by RCG tiles with the higher insulating RCC material present on the nose and wing leading edge regions. Optical properties for RCC and RCG materials have been characterized by Caram ***et al.***[9] and Bouslog ***et al.***[10], respectively. Characterization has mainly concentrated on total hemispherical emissivity because it is critical to understand the heat balance at the surface boundary. However, for the optical measurements, the spectral emissivities in the camera optical bands are required. Furthermore, and in particular for the NIR sensor, the reflectivity in spectral regions for direct and scattered sunlight that fall in these sensor wavebands are also of interest. The RCG spectral emissivities are strongly wavelength dependent below 2 μm. Moreover, those emissivities vary significantly between virgin and flown tiles. Since the CFD temperature maps are not fine enough to provide "tile" level spatial resolution, it is not feasible to track these values on a tile by tile basic. Thus, Fig. 3 shows extracted average curves that are used for the radiance modeling presented herein. Reflectivity measurements for the RCG tiles are not readily available. Therefore, a diffuse reflecting BRDF function is chosen to model radiation reflections.

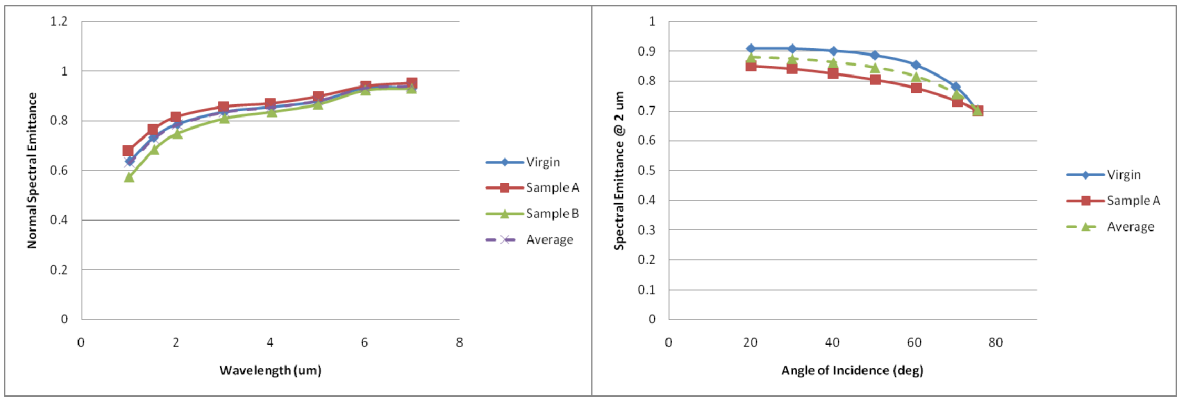

Figure 3. RCG Normal and Directional Spectral Emittance Used for Radiance Modeling.

For the CFD simulations, the total hemispherical emissivities between the RCC and RCG are quite similar so that no distinction is made between them for the surface boundary conditions. This presents some problems for the radiance modeling since there is a notable difference between the material emissivities in the NIR waveband of interest. Since the initial focus was on the DTO wedge region and bulk of the windward surface, the radiance modeling presented herein assumes the total surface is RCG tiles. The effect of this assumption on the preflight radiance predictions will be an underprediction of the radiance, and thus counts, on the nose and leading edge regions. This is not expected to present any difficulties in Cast Glance NIR sensor integration time recommendations. The other effect of this approximation is the overprediction of the surface temperatures by up to about 50°F during the 3-D temperature map reconstruction in these regions.

E. Shuttle Tracks & Orientations

Preliminary reentry trajectories and orbiter attitudes were based on the NASA Entry Flight Dynamics Officer's primary and alternative scenarios for potential landings into Kennedy Space Center, FL, Edwards Air Force Base, CA, and sometimes White Sands Missile Range, NM. To support the preflight radiance modeling, these were converted and read into Satellite Toolkit (STK) software.[17] Nominal Cast Glance Test Support Positions (TSP) were determined by the HYTHIRM mission support team based on desired target Mach number for the data collect, expected orbiter attitude and trajectory, logistics of Cast Glance transit and loiter times, local weather predictions, sun angle, and a number of other factors that can vary in real time. For the radiance predictions, a nominal CG TSP is assumed for a discrete number of target mach numbers (typically one or two per reentry trajectory). The resulting Shuttle position/attitude, Cast Glance position, and date/time are extracted from STK simulations for each case of interest and used as inputs in the FLITES radiance calculations.

Post mission Shuttle trajectory and attitude information was obtained from the Orbiter Data Reduction Center (ODRC).[14] Post mission Cast Glance positions were obtained from onboard recorded information. These flight data are similarly processed through STK to provide information to FLITES in the same coordinate systems as the preflight simulations.

F. Atmospheric Transfer and Backgrounds

Atmospheric effects in the radiance modeling and sensor modeling are handled a couple of ways. Nominally expected atmospheric properties are provided to FLITES which utilizes a standard MODTRAN package[2] to compute the transmission losses between observer and target. In addition, MODTRAN is further used ***via*** an interface graphical code called PLEXUS[15] to provide estimates of the foreground sky in-band radiance. For preflight predictions no clouds were included and a relatively clear "rural 23 km visibility" haze condition was assumed. With Cast Glance flying above much of the lower, denser atmosphere, transmission losses across the standard atmospheric models are typically only a few percent at closest approach. An example of a resulting radiance map is shown in Fig. 1.

For post mission radiance modeling and data analysis, a higher fidelity approach was used which takes into account weather observations over the reentry corridor at the time of the missions. This process is described later in the image processing section.

III. Image Processing and Conversion to 2-D Temperatures

Figure 4 shows a flow diagram of the processing steps used to convert the raw imagery into 2D temperature images of the shuttle. The goal is to produce the highest quality images possible for mapping temperatures onto the shuttle surface. The processing must not contaminate the image numerical values by drastic filtering or reconstruction techniques, which would invalidate the final temperature estimates. The image quality is improved by registering and averaging selected image frames, thereby improving signal-to-noise. Raw image values are converted to radiance values using pre-flight sensor calibration data. Then adjustments are applied to account for atmospheric and emissivity effects. The temperatures are calculated by iterating the Planck blackbody function over the optical filter waveband. The temperature calculation is essentially the reverse process of the radiance modeling that was used to estimate expected image values as described in the previous section. The following sub-sections will describe each of these image processing steps in more detail.

A. Image Acquisition

The imagery acquired by the US Navy's NP-3D Orion as well as a description of its Cast Glance long-range optical sensor package is detailed in Refs. 5 and 6. In brief summary, a Prosilica GC1380 CCD camera (1024 x 1024 pixels) with an 850nm cut-on filter was used to collect imagery in the near-infrared region. The Cast Glance optical path uses a gimbaled mirror for pointing and provides a field-of-view of approximately 0.215°, diagonal.

At a nominal range of 35 nmi each pixel subtends approximately 0.78 feet. A shuttle is 122 feet in length, so detailed imagery comprising more than 100 pixels along the Shuttle projected length is acquired during closest approach to the aircraft. However, as noted earlier, degradation of the optical system's point spread function due to the atmospheric blurring as well as jitter and unresolved motions, the resolution limit of the acquired imagery is estimated to be approximately 3 feet at 35 nmi range.

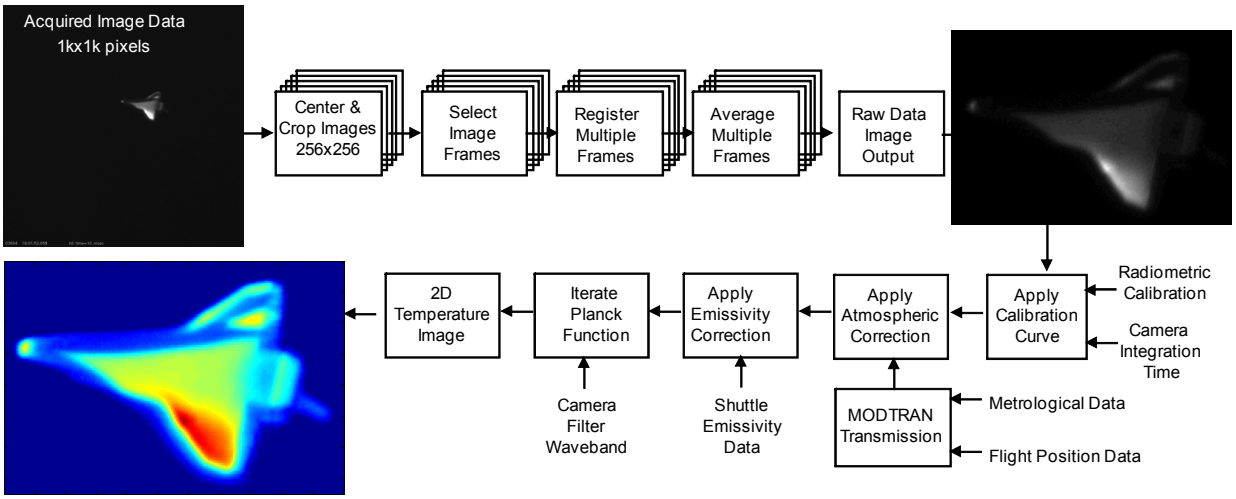

Figure 4. Processing steps to compute a 2D temperature image.

Tracking of the Shuttle during image acquisition was done manually by experienced personnel as is detailed by Tack ***et al.***[5] The Cast Glance team was able to keep the Shuttle within the image field-of-view during the data collection despite the high angular rates near closest approach.

B. Center and Crop Images

Because of the aircraft motions and vibration, as well as the high velocity of the shuttle, several steps were required to minimize the detrimental effects of frame-to-frame image motion, blurring and jitter. These steps, shown in the top row of Fig. 4, markedly improve the signal-to-noise of the imagery while maintaining image quality. The first issue to be remediated is that the Shuttle changes position from frame-to-frame, which requires the image centering step described below.

We begin cropping each image to 256 x 256 pixels. As mentioned, even at closest approach, the shuttle will cover slightly more the 100 image pixels along its length, so a 256 x 256 image is easily large enough. The centering process relies on careful segmentation of the Shuttle from the background and then calculating the geometric centroid. Segmentation of the shuttle is not trivial because the following key elements vary during the image sequence: 1) Shuttle orientation, 2) image intensity levels of the background, and 3) image intensity levels of the Shuttle. Completing the centering and cropping step well provides frame-to-frame matching to within a couple of pixels, but not much better. Further frame-to-frame image registration is applied later. However, this centering and cropping step greatly reduces the computational load for later processing and eases image analysis.

C. Image Selection

The next step is to select the best image frames within the thousands of image frames that were acquired during several minutes as the Shuttle approached and flew past the Cast Glance aircraft. There are two different aspects for this step: 1) determining the best range of image frames (time range), 2) selecting best frames within that time range.

The first aspect of image selection is to determine the time range during acquisition that had the best view of the shuttle surface. After using the method in the previous section to segment the shuttle from the background, the total number of pixels on the Shuttle surface is computed for each image frame. The range of image frames with the highest number of pixels can indicate the most broadside view. This was also confirmed by calculating the angle between the line of sight and Shuttle body z-axis, which was at minimum during the same image frames as indicated by the maximum pixels on the Shuttle.

The second aspect of image selection is choosing the best images available within the optimal time range. As mentioned previously, image motion and jitter are the main causes of blurring. For a manually-tracked image sequence there are often major differences in the image quality frame-to-frame. Some image frames can be better in quality than most frames, while other frames are too blurred. For our situation, several “point-like” and “line-like”

features on the shuttle were examined to assess blurring. For example, the leading edges of the wings should form sharp edges whereas the nose should appear point-like. We have also found that the body flap can exhibit well defined edges with intensity values much higher than the background. To maintain the highest possible image quality, a majority of frames were actually discarded from further processing. Typically, one-third of the frames within the range of frames with maximum pixels on the shuttle were selected for subsequent steps. We note here that a similar but more extensive discussion of image selection has also been presented by Zalameda ***et al***.[6]

D. Register Multiple Frames

Proper registration of multiple frames is critical to not reintroducing blur, thus maintaining the quantitative image quality found in each frame of the hand-picked data set, and achieving the statistical gains of co-adding. The registration process carefully aligns the images so that corresponding image locations are within the same pixel.

Image registration is a large field of study and therefore many methods and techniques have been developed. For this application, two methods were considered: 1) feature-based, and 2) intensity-based. For feature-based methods, corresponding features (or landmarks) are selected in the images and a linear transformation transform (translation, rotation, scaling) is applied in order to overlay the selected features in the images. Several registrations were completed using six manually-selected landmark points on the Shuttle and then the linear transformation applied. Results were good, however, landmark selection is highly sensitive to the accuracy of point selection, and it is too tedious to complete for multiple data sets.

For intensity-based methods, the entire intensity data in the images is used to estimate the linear transformation, allowing for some local nonlinear distortions in geometry. These methods are generally automated, although the characteristics of the data can sometimes influence the results. Although a comprehensive evaluation of the many techniques available could not be done within the time constraints, the technique that performed best for the HYTHIRM imagery was taken from a medical imaging application developed at Dartmouth College[3,16]. The transformation between images is modeled as locally affine but globally smooth, and it explicitly accounts for local and global variations in image intensities. The algorithm is built upon a differential multi-scale framework. For the frame-to-frame variations in the imagery due to point spread and atmospherics, and passable jitter, this registration algorithm proved well-suited to account for these variations and provide excellent alignment.

E. Average Multiple Frames

After multiple images are registered to a single image, they are averaged to improve image statistics if not quality. If well selected, the image signal-to-noise ratio will typically improve as the square of the number of image frames averaged. In our case the results of averaging from 9 to 49 frames were compared, and the performance benefit was found best for about 25 frames. This evaluation was completed through visual comparison of zoomed image features, as shown in Fig. 5 (for STS-119). The top two images show a cropped single frame of the Shuttle and a zoomed section of the starboard wing. The lower two images show the same image portions after 25 frames were registered and averaged. The pixel variations are markedly reduced and the edges appear sharper.

F. Apply Calibration Curve

Calibration data were acquired and processed for these observations as described in Ref. 6. The primary result of the calibration is an equation that converts raw intensity counts at the sensor into a radiance value in ($W\ cm^{-2}\ sr^{-1}$), scalable with integration time. This conversion is applied to the improved image (the image after registration and averaging) to obtain a radiance image. The foreground radiance (i.e., atmospheric radiance, not from the Shuttle) is estimated at several locations within the image and then subtracted from the radiance image to obtain an averaged estimated radiance from the Shuttle, without needing to account for transmission loss through the atmosphere. The transmission loss is described in the next section.

G. Apply Atmospheric Correction

A small transmission loss occurs in the atmosphere due to the scattering and absorption along the path from the Shuttle to the sensor. An instantaneous transmittance value is calculated using MODTRAN with inputs of the observing geometry and the best available atmospheric data in the near vicinity at the image acquisition times. The atmospheric data were taken from the Air Force Weather Agency's 3D model and were collected within the nearest

hour of the data collection. The spectral band used of the previously noted sensor top-hat response (flat) from 0.843 to 1.1 microns

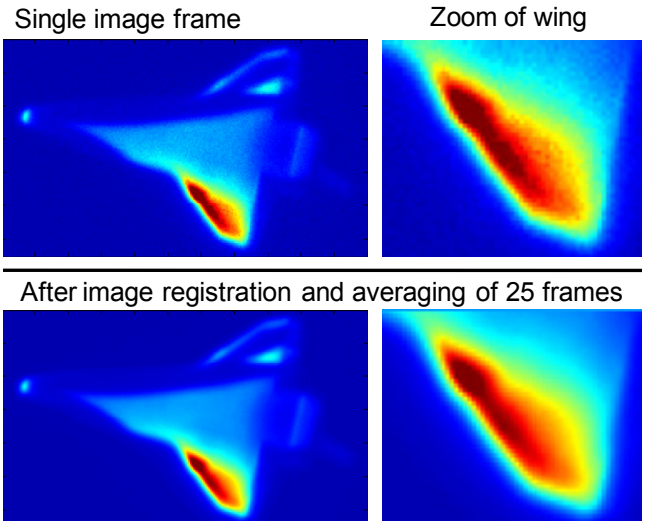

Figure 5. Example of image quality improvement for STS-119 after image selection, registration and averaging of 25 frames.

For each image frame time, the average in-band transmittance is then computed. During early images the line-of-sight has a lower elevation and goes through more of the atmosphere, thus the transmittance is lower. Near closest approach, the line-of-sight is at a higher elevation (more upward), so the transmittance is higher. For clear conditions and a nominal 35 km range, the transmittance usually reaches approximately 0.97 for closest approach. This 3% transmission loss is relatively small, but it must still be included to correctly estimate that shuttle feature brightnesses and ultimately temperatures.

H. Apply Emissivity Correction

The emissivity of the materials on the shuttle surface is reasonably well known, however it varies depending on the material type, RCG or RCC. Since it is difficult to classify each image pixel as one particular material, we have chosen an emissivity of the entire shuttle to be 0.61, characteristic of RCC the type of tile used on most of the shuttle's windward surface and the typical observing geometry. In this way our calculations will be relatively accurate, except for the nose and wing edges, where there is also more uncertainty due to point spread. The calculated radiance is divided by the emissivity to adjust to a blackbody equivalent value, which is necessary to convert to a temperature.

I. Iterate Planck Function

The radiance is given by the Planck blackbody radiance function. Therefore, the temperature at each pixel is calculated by iterating the Planck function within the top-hat response from 0.843 to 1.1 microns. An initial temperature is given to calculate an initial radiance, and the difference between the pixel radiance and initial estimated radiance is determined. The iteration of estimating the temperature and computing the radiance continues until the difference with the image pixel radiance is below a specified tolerance, about 1%.

J. Uncertainties of Temperature Estimates

The final temperature image is a result of a series of calculations, most of which have uncertainties. It begins with the uncertainties of the sensor measurements, ***i.e.*** pixel counts. Because we are co-adding about 25 frames of well exposed digital imagery, noise statistics are unlike to account for more than 0.5% error. Uncertainties in estimating the atmospheric effects are more difficult to estimate but they too are likely to be very small (<0.5%) given that

relatively little absorption and scattering can occur above aircraft altitudes provided that the skies are at all clear. Even for STS-119 this was the case at higher elevation angles. Calibration errors can contribute at most 2% [Ref. 6]. But, it is our use of an emissivity value of 0.61 that is the approximation with the greatest uncertainty, about 7%. In addition, a lack of knowledge of the effective point spread function contributes some uncertainty to the measurements at the Shuttle edges and regions where spatially the intensity changes most rapidly. To quantify these uncertainties in these areas would be extremely difficult. However, in the middle of the Shuttle's lower surface the above estimates of uncertainty add in quadrature, thus leading to a radiance error estimate of approximately 7.5%.

However, since the radiance is roughly proportional to T^3 on the Wein side of the blackbody curve – our case – the corresponding temperature errors are unlikely to be greater than 2% to 3%. This compares favorably with the +/-5% agreement achieved in the earlier ISAFE work for STS-96.[13] And that is the great power of this NIR temperature measurement technique (as will be demonstrated later when the radiatively determined temperatures are compared Shuttle thermocouples measurements and the CFD temperature estimates).

IV. 3-D Surface Temperature Mapping

In this section, we describe the optimization process used to provide 3-D surface temperature maps on the Shuttle orbiter surface. Both the radiance modeling and processed NIR imagery are utilized to provide a consistent estimate of the surface temperatures at the point of near maximum spatial resolution on the windward surface. A difficulty in the process is that the temperature spatial gradients and geometry scales on the orbiter are, in general, finer than the optical sensor resolution. Thus, the mapping process herein will provide a surface temperature distribution that is consistent with the observations, but not necessarily a unique solution. The effects of this will be discussed with the results presented for the STS-119 mission.

A. Schema: Match the Observed Radiance using Temperature as a Local Variable

The basic procedure used to estimate the 3-D temperature maps follows a Newton's Method approach. First, a "simulated temperature map" is "guessed." To begin, initial temperatures are assigned to a large number of nodal points on the surface and an APL radiance model (***i.e.,*** a FLITES-type radiance map) is computed. Comparison of the simulate radiance map with the calibrated, processed and registered CG NIR data at an instance in time yields differences that inform temperature deltas for the next iteration, and so on. This provides a convergence of a radiance field in "pixel" space.

B. Methodology particulars

Before estimating the surface temperatures for the mesh, the surface grid must first be mapped to image pixels. Here, it is important that the fractional contribution that each surface vertex contributes to each pixel is proper accounted for. Fortunately this is just what the APL radiance model does.

Because of optical blurring and arbitrary alignment of surface mesh facets with image pixels, each mesh vertex generally lies in multiple neighboring pixels. To mitigate errors it is necessary that the computational mesh be at a much higher spatial resolution of than the optical resolution. Here, the 3-D surface mesh used for the 3-D temperature mapping consisted of 15,216 nodes. This number was derived by reducing the CFD computational mesh by a factor of four in both 'i' and 'j' directions. Then, as a part of the Newton's Method approach, temperature increments, dT, for each pixel are estimated to converge the radiance fields in pixel space. The pixel-to-vertex mapping allows the creation of a list of dT's for each grid vertex. Thus, the actual temperature adjustment applied to a particular vertex is a weighted average of the pixel dT's to which it contributes.

Figure 6 shows an example of both the processed data imagery and a converged radiance model for the point near closest approach for the STS-119 mission. Clearly, the schema adopted succeeds in producing at least one model that well represents the actual data. But is the computed temperature map a true representation of the actual one?

C. Computed Temperature Map and Accuracy

Figure 7 shows two views of the converged 3-D temperature map for STS-119 at closest approach that produced the radiance model above. The thermograph to the left is placed in the orientation actually observed. In examining

this first (and as yet only) computational thermograph, one notices some spatial oscillations in temperature where "smooth" variations be expected. In addition there appears to be "ringing" effects at the wing leading edges. These are believed to be numerical artifacts related to the 3-D mesh being much finer than the NIR optical resolution for this case. We note here that while subsequent maps may show aesthetically more pleasing representations all estimated thermographs are just that . . . estimates. And these estimates are subject to error in large part because the point spread function – a highly variable product of both seeing and aircraft vibrations – is difficult (though not impossible) to estimate for any one frame much less a collection of frames.

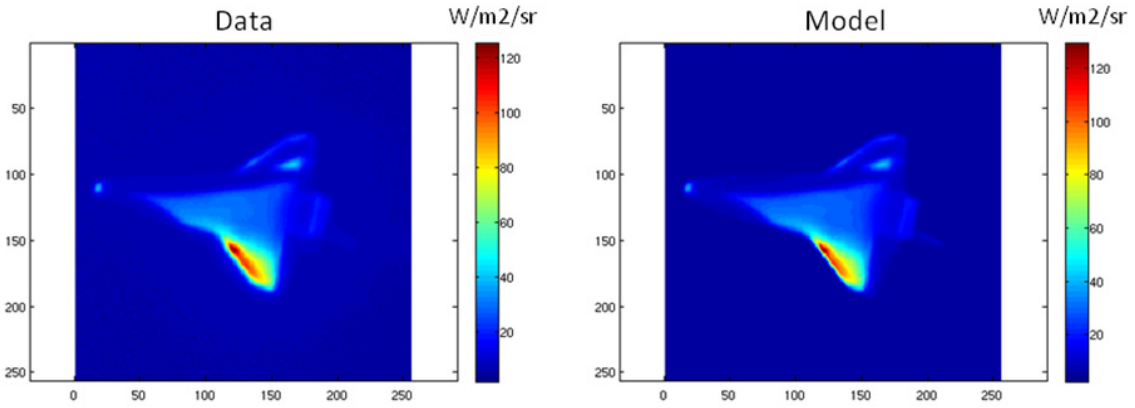

Figure 6: Comparison of the radiance maps between the STS-119 processed imagery centered on frame 3664 and the final radiance map from the converged 3-D temperature mapping.

At the time of this writing, we can only estimate the accuracy of our initial thermographic measurements by noting how in the series of iterations leading to the "final map" the temperatures "converged" to their final estimates. In essence these are internal statistical error estimates and do not include the sensor and calibration errors noted in Ref. 6. Nevertheless, these internal error values are very low, typically in the range of 10°F to 20°F rms. We expect these error estimates to be refined with additional analyses.

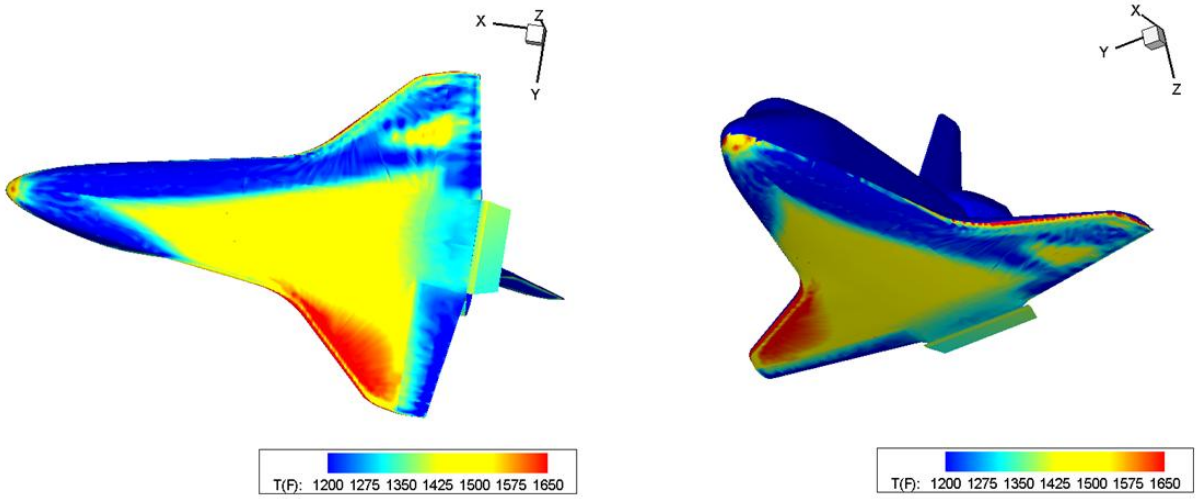

Figure 7: 3-D surface temperature map for STS-119 corresponding to frame 3664 (GMT 19:01:52.658). The observed orientation is shown to the left. A representation that better shows the actual curvature of the windward surface is shown to the right.

V. Mission Results

Three sets of imagery have been processed:

1) STS-119: Shuttle Discovery was observed from 51.9 km while at Mach 8.43.
2) STS-125: Shuttle Atlantis was observed from 70.9 km while at almost Mach 14.33.
3) STS-128: Shuttle Discovery was observed from 79.6 km while at Mach 14.73.

Table 1 lists the basic information from each mission for comparison and reference. In the following subsections we present the temperature image for the listed frame and GMT together with a discussion of the results.

A. STS-119

STS-119 Discovery was equipped with a 0.25 inch wing protuberance to induce turbulence in a portion of the aft port wing. The Shuttle de-orbited on revolution 202 and during re-entry passed over the southeast portion of the Gulf of Mexico where the imaging encounter occurred. It was approximately 3:00 pm local time with scattered cirrus clouds in the region.

Table 1: Information Related to Processed Imagery from Each Mission

Mission	STS-119	STS-125	STS-128
Date	28-MAR-2009	24-MAY-2009	12-SEP-2009
Image Frame Number	3664	6372	6261
GMT	19:01:52.658	15:24:33.473	00:38:46.057
Line-of-Sight Distance (km)	51.9	70.9	79.6
STS velocity (mach)	8.43	14.33	14.73

Figure 8 shows the processed temperature image for GMT 19:01:52.658. The higher temperatures from the wing protuberance are easily observed on aft port side. There was another unanticipated transition to turbulent flow event observed during re-entry. The turbulence occurred asymmetrically across most of the Shuttle's lower starboard surface and is often referred to as an Asymmetric Boundary Layer Transition (ABLT). The ABLT appeared to arise in proximity to the forward nose wheel doors although a precise surface defect in the tiles was never determined post landing. The ABLT resulted in higher temperatures along the entire starboard side, especially near the leading edge of the wing, and widened to the aft center along the Shuttle. The development of this ABLT was observed long range and is described in more detail in Ref. 4.

One "unexpected" result was the significant brightness of the body flap. As noted earlier this control surface had not been included in any of the CFD temperature maps provided to the modeling team.

B. STS-125

The STS-125 mission was not equipped with a DTO protuberance, so nominal laminar flow was expected at the Mach numbers of interest to HYTHIRM. The Shuttle was flying into Edwards AFB on revolution 197 during data collection. It was approximately 7:00 am local time with relatively clear skies in the region. Sun glare became increasingly strong as the shuttle-Cast Glance-sun angle narrowed as Discovery was viewed to the East.

Figure 9 shows the processed temperature image for GMT 15:24:33.473. The Shuttle was at Mach 14.3 at this point so the temperatures are higher than for STS-119 at Mach 8.4. Elevon gap heating is evident, but otherwise the Shuttle surface temperatures were as predicted.

C. STS-128

The STS-128 mission was equipped with a 0.35 inch DTO wedge to induce turbulence in the same aft portion of the port wing as STS-119. The Shuttle Discovery flew into Edwards AFB on Rev EDW-219 during data collection. It was approximately 6:00 pm local time on September 11, 2009 with clear skies above in the vicinity of the aircraft. Remnants of Hurricane Linda were not far to the Southwest but all clouds were well below the aircraft altitude.

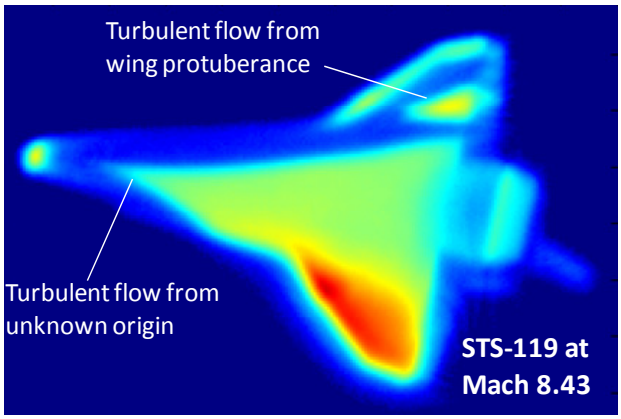

Figure 8: Radiometrically calibrated temperature image for STS-119 derived from processing imagery with center point at frame 3664 (GMT 19:01:52.658).

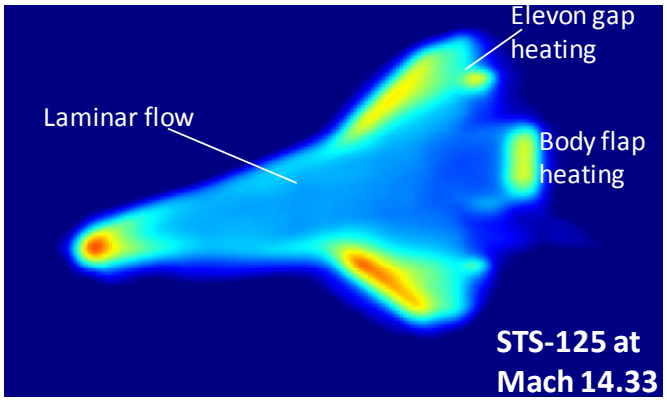

Figure 9: Radiometrically calibrated temperature image for STS-125 derived from processing imagery with center point at frame 6372 (GMT 15:24:33.473).

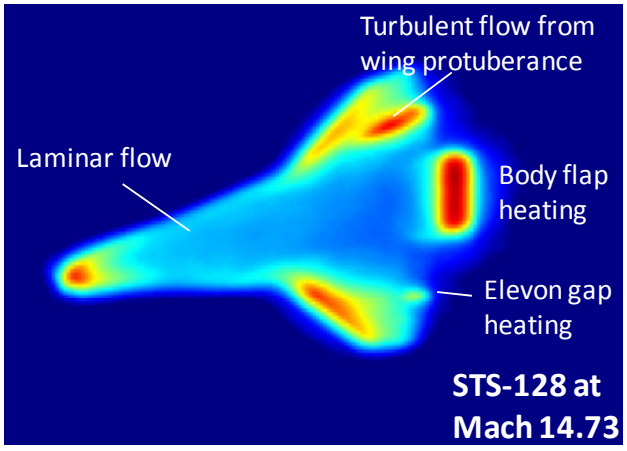

Figure 10: Radiometrically calibrated temperature image for STS-128 derived from processing imagery with center point at frame 6261 (GMT 00:38:46.057).

Figure 10 shows the processed temperature image for GMT 00:38:46.057 on September 12. The Shuttle was at Mach 15 at this point so the temperatures are higher than for STS-119 (at Mach 9) but similar to those for STS-125. Comparison with STS-125 shows the wedge-induced turbulence at the port aft wing to be quite obvious. It does have a narrower wedge angle than STS-119's due to the higher mach.

Elevon gap heating on STS-128 appears similar to that observed on STS-125, however the body flap appeared much warmer. As expected, the higher surface temperatures measured on the on the STS-128 body flap were the result of a larger deflection angle of 7.5°, relative the STS-125 body flap at 1.9°. Unfortunately, the body flap thermocouple was not operating during Atlantis' STS-128 re-entry so it was not possible to compare the higher remotely-observed temperatures with a discrete TC measurement.

VI. Comparison to Thermocouple Measurements

Thermocouples were placed within Shuttle tiles at several locations, thus permitting comparisons with the optically-determined 3-D thermographic temperatures. However, it is important to note that the sensors themselves were not surface-mounted but rather embedded slightly within the tile. So if there is a slight temperature change between the surface and sensor, comparisons should include this bias. Experts within the Shuttle program have suggested that a thermocouple measurement should be approximately 20°F lower than the corresponding surface temperature.[4] Thus we add 20°F to the thermocouple values before comparison to surface temperatures estimated from the NIR imagery, just as was done by other HYTHIRM analyses.[8] As discussed by Zalameda ***et al.***[6], there is some uncertainty in the thermocouple measurements that is still being characterized. However, these thermocouple measurements are good reference points for comparison to the temperatures estimated from the NIR imagery.

The locations of the thermocouples are known for each mission; however the corresponding image pixel locations must be determined – for both 2-D imagery and 3-D thermography – if comparisons are to be made accurately. In the former case, this was accomplished by approximating the pixel dimensions based on the distance from the sensor to the Shuttle and the appropriate scaling due to off axis view of the Shuttle surface. At the best estimated location in the imagery corresponding to the thermocouple location, a single pixel value and an average of a 3x3 pixel region was computed. A comparison is presented for STS-119. Data for STS-125 and STS-128 will presented at a later date. For the 3D temperature mapped data, the thermocouple location is applied directly to the corresponding 3D model location.

Figure 11 shows nominal thermocouple positions and the measured temperatures at the center time of the optical measurements (GMT 19:01:52.658). The temperature estimates from the imagery were typically higher than those measured by the thermocouples. The average deviation from the thermocouple was about 92°F, which is less than 10% of the measurement value. On face value this alone would lend credence to the use of NIR image thermography for Shuttle temperature estimates. But that is not the whole story.

The two most deviant measurement comparisons, those from thermocouples 9468 and 9480, would seem to have observational if not physical explanations. Both thermocouples were located near the edge of the turbulent region, and their values were much lower than the temperature estimates from the imagery. It seems possible that the blurring (point spread) of the turbulent region was enough to "bleed" into the locations where the thermocouples are located in the imagery, perhaps do to an injudicious choice for the point spread function. It may be that the thermocouple is actually located just outside of the turbulence, yielding a lower thermocouple measurement. If thermocouples 9468 and 9480 are not included in the statistics, the differences from the imagery of the other four thermocouples averaged only about 37°F (<2%). These differences are consistent with the errors estimated in §III-J above.

Going one step further it is fair to say that the largest apparent deviations occur where the temperature gradients appear largest. Better observations and/or better estimates and use of the point spread function will undoubtedly narrow that gap. But the question of whether the two temperature measuring techniques are actually measuring the same phenomenology needs to be asked. Is it possible that higher temperatures exist in a layer of heated air above the tiles? Such a theory would explain the higher optically-determined temperatures above thermocouples 9468 and 9480 since hotter air would be seen in projection above their positions. We know this hotter air exists at measureable optical values since it is seen in the wakes behind the shuttle.[6]

For STS-119 Discovery, thermocouples were strategically place downstream of the protuberance on the aft port side wing. Six of the active thermocouples were placed almost linearly along a cross-section of the turbulent wedge region TC#1, 3, 8, 6, 4, 7). Figure 12 shows the thermocouple locations and the temperature comparisons within the turbulent wedge region.

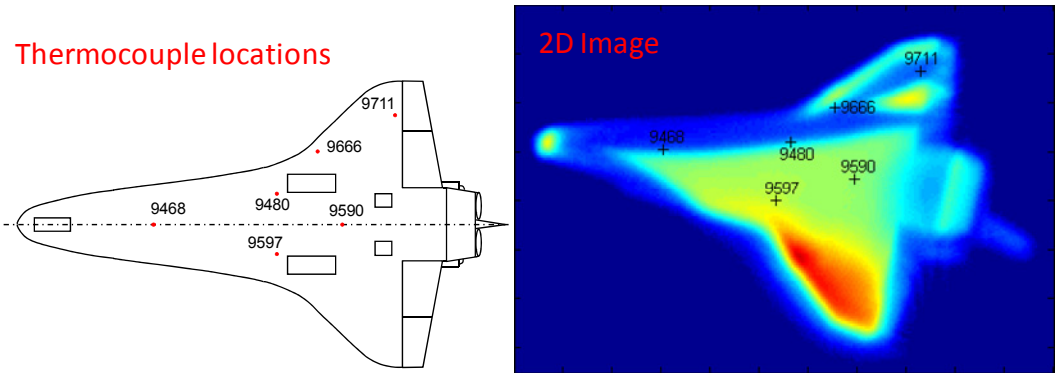

Thermocouple ID	Thermocouple + 20 (F) {TC}	2D Image Temperature Estimate(F) {TE}	Temperature Difference(F) {TE - TC}	Temperature Average in 3x3 pixel area (F) {TA}	Temperature Difference (F) {TA - TC}	3D Model Temperature Estimate(F) {TE3}	Temperature Difference(F) {TE3 - TC}
9468	1092	1258	166	1258.8	166.8	1382	290
9480	1063	1302	239	1303.4	240.4	1306	243
9597	1509	1492	-17	1493.3	-15.7	1489	-20
9590	1450	1461	11	1459.7	9.7	1451	1
9666	1257	1309	52	1312.9	55.9	1322	65
9711	1176	1243	67	1244.8	68.8	1200	24

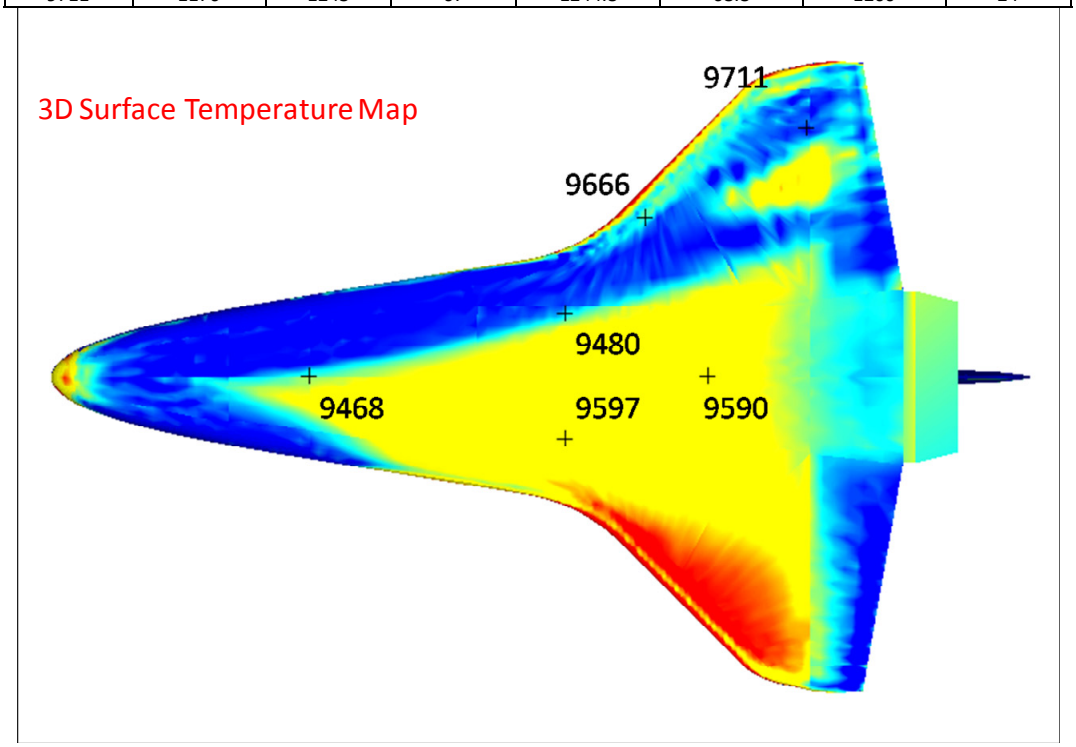

Figure 11: Shuttle diagram with nominal thermocouple locations placed in Discovery STS-119. Table with thermocouple measurements and temperature estimates from imagery at GMT 19:01:52.658. Thermocouple data are taken from Wood ***et al.***[8]

A vertical line profile crossing the wedge region in the imagery is shown representing the locations for the temperature profiles. Compared to thermocouples (1,3,8,6,4,7) along the line profile, the imagery showed a blurring effect similar to a low pass filter. This is expected for high gradient regions within the imagery. The thermocouples showed a sharp transition from slightly above 1100°F to almost 1700°F within about 30 inches of separation. In the imagery, the temperature transitions were not as sharp or as high.

As shown by Fig. 12, these thermocouples were very closely spaced and were within a more spatially dynamic region of temperatures. Although the imagery does not have the resolution necessary to effectively compare to these closely spaced thermocouples, the imagery does provide good qualitative information in the DTO region.

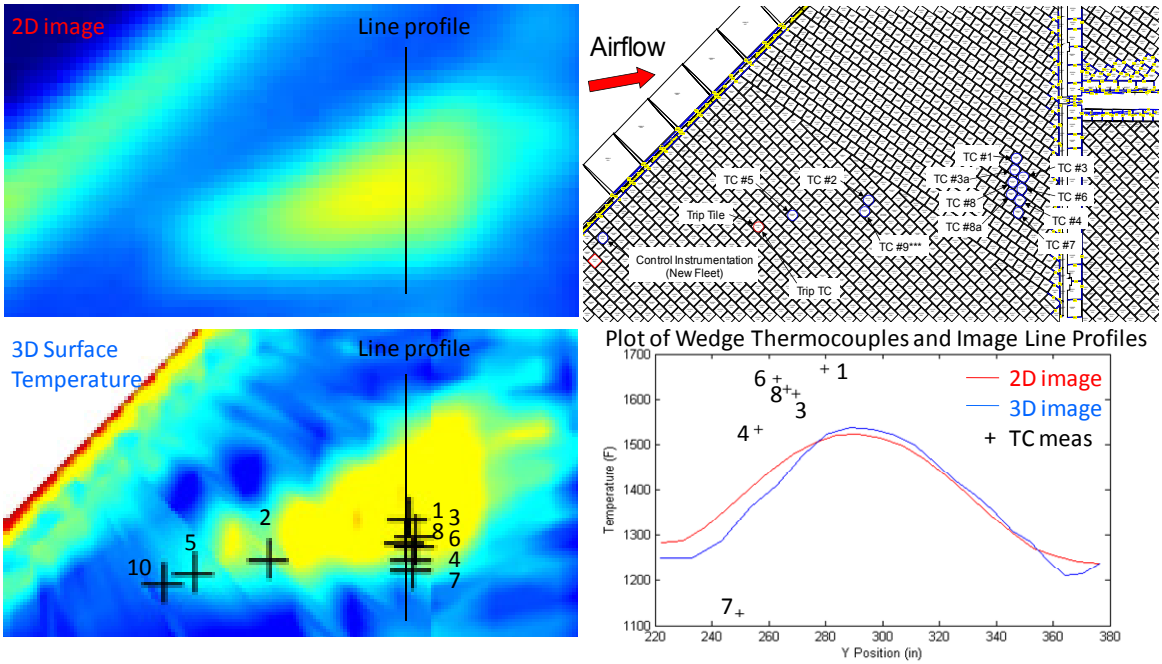

Figure 12: Comparison of temperatures in the DTO wedge region. Upper right is portion of shuttle port wing with DTO thermocouple locations placed in Discovery STS-119. Upper left is zoomed region of 2D temperature image at GMT 19:01:52.658. Lower left is zoomed region of 3D Surface Temperature map and overlaid thermocouple locations. Here, the opening angle of the wedge appears to be 21° ± 2° on an axis inclined 17° ± 1° to the center line. Lower right is plot of temperatures along the line profiles in the imagery and the six thermocouple values along the line profile.

VII. Conclusions and Next Steps

We have gone full circle to provide the first geometrically accurate (i.e., 3-D) temperature maps of the entire windward surface of the Space Shuttle during hypersonic reentry. We took estimated surface temperatures derived from CFD models at integral high Mach numbers and used them, the Shuttle's surface properties and reasonable estimates of the sensor-to-target geometry to predict the emitted spectral radiance from the surface (in units of W sr^{-1} m^{-2} nm^{-1}). These data were converted to sensor counts using properties of the sensor (e.g. aperture, spectral band, various efficiencies, and the calibration), the expected background, and the atmosphere transmission to inform the optimal settings for the near-infrared and midwave IR cameras on the Cast Glance aircraft. Once these data were collected, calibrated, edited, registered and co-added we formed both 2-D maps of the scene in the above units and 3-D maps of the bottom surface in temperature that could be compared with not only the initial inputs but also thermocouple data from the Shuttle itself.

The results go well beyond remarkable. For the only case that has been "fully" analyzed, STS-119, we have confidence that the internal accuracies of the temperatures estimates are better than 2% rms, provided the local temperature is above a minimum threshold of about 1200 °F (to which the sensor responds well) and the region is not one with sharp temperature gradients. Unfortunately, the DTO wedge is such a region. Without improved optical resolution it will be difficult to markedly improve upon the accuracy of the temperature maps in the wedge in the near future. Unfortunately, airborne optical systems with both better high speed tracking capabilities AND better effective resolution (which includes the mitigation of jitter) than Cast Glance are not currently available. We are confident that some improvements can be made in obtaining a better understanding of the "effective point spread function" which will accommodate both image wander and vibration-induced image spread. These improvements can then be fed into the 3-D temperature mapping technique which itself can also be improved to lessen the low level "ringing" (i.e. the "mottled" appearance of the maps seen in highest resolution which is due to the iterative technique used), which most adversely affects high-gradient regions like the wedge.

What we can say with certainty is that the HYTHIRM team has successfully demonstrated the efficacy of using NIR imagery to map the Shuttles' global temperature structure during hypersonic reentry – the program's primary goal. We have further demonstrated that the accuracy of NIR-determined temperatures is relatively insensitive to errors in the measurements and the calibration, and in certain circumstances appears to be on par with the accuracies of the thermocouple measurements.

VIII. Executive Summary

High-resolution, calibrated near-infrared (NIR) imagery of the Space Shuttle obtained during the STS-119, STS-125 and STS-128 hypervelocity atmospheric entries has provided information never before observed on the distribution of surface temperatures and the state of the airflow over the entire windward surface of the Orbiter. On Space Shuttle Discovery's STS-119 and STS-128 missions, NASA flew a specially modified tile on the Orbiter's port wing designed to induce laminar to turbulent boundary layer transition at Mach 15 and Mach 18, respectively. The tile featured a four-inch wide "trip" or "speed bump" which measured 0.25 inches high on STS-119 and 0.35 inches high for STS-128. In conjunction with Discovery's standard thermocouple instrumentation, this particular Orbiter was augmented with an enhanced distribution of 10 surface thermocouples aft of the trip to monitor local downstream heating effects. Collectively, these discrete measurements provide ground truth for the remote optical measurements. STS-125 (Atlantis) was not configured with a wing protuberance (or the augmented thermocouples) and, therefore, provided temperature measurements associated with a a high Mach laminar flow. A full description of the on-board experiment package as well as the motivations for its employment for flight thermography can be found in Ref. 7.

Hypersonic Thermal Infrared Measurements (HYTHIRM) of the Shuttle reentries were made from a US Navy NP-3D Orion aircraft equipped with a long-range infrared optical package referred to as Cast Glance. Its NIR imaging sensor, a band-limited CCD behind a sophisticated, agile tracking mount and telescope, was calibrated prior to the first mission and recalibrated before the third. These calibrations were not only essential to our ability to convert from counts to observed irradiance and, ultimately, to temperature maps, but also our ability to predict optimal sensor integration settings from predicted temperature distributions supplied before each mission. The airborne instrumentation is described in Ref. 5 together with observational and logistical summaries for each mission. The application of the NIR sensor is further described in Ref. 6.

In this paper, we first describe in detail the model that was developed to predict Shuttle spectral irradiances at Cast Glance. Based on a DoD code named FLITES, the HYTHIRM Radiance Model takes as its principal input a NASA-supplied wireframe temperature map appropriate to a specific (usually integral) Mach number. The conversion to sensor counts takes into account a number of observational-, time-, and/or environmental-specific variables including: shuttle tile properties (emissivity and reflectivity, all Shuttle location-, temperature-, and view-angle-specific); Shuttle orientation; the Shuttle-Cast Glance viewing geometry; atmospheric radiative transfer models including the effects of sun- and earthshine; and the sensor model. The sensor model also approximated the optical systems' expected resolutions. The outputs from the radiance models were used pre-flight to optimize the NIR and mid-wave infrared (MWIR) sensor integration times. This assured that raw data would be collected that would span each sensor's maximum dynamic range, while still mitigating against saturation.

We also describe our post-mission image processing methodology which emphasized corrections on an image-by-image basis to assure that accurate Shuttle surface spectral radiances have been determined and accurate surface temperatures calculated. In particular, a rigorous analytical image registration method was applied post-flight to remove geometric effects of non-orthogonal projections on the image plane. That is, 2-D pixel coordinates were projected onto the lower surface of the Shuttle using flight orientation information from both the Shuttle and the Cast Glance aircraft at the time of image acquisition. Next, the "final" 2-D temperature images are "projected" onto the Shuttle's windward surface. Once the temperature is properly aligned and adjusted for geometric effects comparisons can be made to surface temperatures measured by Shuttle surface thermocouples.

Three sets of imagery have been processed thus far: 1) STS-119 when Shuttle Discovery was as close as 28 nmi while at Mach 8.4 and 160 kft ; 2) STS-125 when Shuttle Atlantis was observed from a minimum distance of 36 nmi while somewhat higher and considerably faster at Mach 14.3; and 3) STS-128 also imaged at approximately 30 nmi at Mach 14.7. Challenges presented in processing a manually-tracked high-angular rate, air-to-air image data collection included management of significant frame-to-frame motions, motion-induced blurring, daylight conditions, as well as changing sky backgrounds (including some cirrus), orientations, and ranges. By reducing the detrimental effects due to motion (sensor and Shuttle), vibration, and atmospherics for image quality improvement, we were able to maintain the quantitative integrity of the data, especially local intensity variations. Our approach was to select and utilize only the highest quality images, register as many co-temporal image frames to a single image frame as changing conditions would allow, and then add the registered frames to improve signal-to-noise, image resolution, and dynamic range.

Weather satellite data, ground-based soundings and atmospheric models were all used effectively to correct the imagery for absorption and lighting effects as the lines of sight quickly changed. And as mentioned earlier, the processing of the thermal imagery was also made difficult because all of the reentries were observed in full daylight. In the case of STS-125 the early morning sun directly illuminated the bottom surface of Atlantis in contrast to STS-128 where a late afternoon sun directly illuminated only the top and sides of the Orbiter. STS-119 was illuminated from above by a mid-afternoon sun. In addition, those observations were made through a thin cirrus cloud deck, which not only provided spatially variable foreground irradiance and signal extinction but also effectively degraded the image resolution.

In addition to the "2-D image analyses and temperature determinations" reported above we also introduce a novel way to determine the 3-D temperature distribution on the Shuttle's windward surface in order to make comparisons with hydrodynamic models more direct and insightful. Instead of converting the registered and averaged image counts directly to temperatures using preflight calibration data, we have used the FLITES-based radiance model in an iterative fashion by first "guessing" the temperature distribution and then determining the "expected" sensor count distribution. These "pseudo-raw images," which include all of the physical and geometrical effects mentioned earlier can then be compared directly with the observed images. Early in the process, local differences between the pseudo and real images inform corrections to the local temperatures for the next "Newton-type" iteration, and so on until the global image "converges." This process has two distinct advantages. First it allows the stronger emissions from the hotter surfaces to influence the entire image ***via*** the effective point spread function (psf). Second, the rate of convergence informs us on the uncertainties of our temperature estimates. The latter is extraordinarily important when comparing these remotely-determined global temperature distributions with the localized thermocouple measurements done here in this study.

As anticipated, the imagery from STS-125 showed smooth spatial and temporal variations across the bottom surface indicative of laminar flow. Only on Atlantis' nose, its wing leading edges, and in the regions of the aileron and aft ramp splits, do shock effects drive the temperatures significantly higher. These results might be unremarkable were it not for the fact that this was the first time such determinations have been made globally in the laminar flow regime at such a high Mach number.

STS-128, observed at approximately the same Mach number as STS-125, provided a more complex picture since Discovery carried the 0.35" high trip. Turbulence in the wake behind the trip was observed to increase the Orbiter's surface temperatures locally by more than 350°F over those in comparable laminar flow regions on the starboard wing. These remotely determined boundary layer transition (BLT) temperatures will be compared with those measured by surface thermocouples[8] at a later date.

Although it was the actually first of this series of reentries to be observed, STS-119 provided the most complex and visually arresting results. The "trip" on the port wing produced a fully turbulent wake, as expected. What was not expected was the asymmetric boundary layer transition (ABLT) that originated near the nose and spread over

Discovery's entire starboard side. But it was also for STS-119 that the 3-D temperature mapping technique was first used to estimate a temperature distribution. Not only can this distribution match the observations (demonstrating internal consistency) but it is remarkably similar to the CFD models.[8,12] And where it significantly differs from the thermocouple data it does so in regions where the temperature gradients are largest, ***e.g.***, in the region of the DTO wedge. The lesson learned, an expected one, is that optical resolution is the key to the realm when attempting to determine the global temperature distributions of hypersonic vehicles from remote NIR imagery. When it is sufficient, as it is for the case of the STS-119 Space Shuttle ABLT, the flight thermography is both spectacular and highly informative.

IX. Acknowledgments

The APL authors particularly wish to acknowledge the critical contributions of their colleagues Kwame Osei-Wusu, Dr. Michael A. Kelly and Doug Holland to our data collection and processing efforts. These gentlemen scholars used cloud-free line-of-sight software developed for another program to support the HYHIRM mission weather decision process. The timely use of this software gave confidence to, if not made possible, the HYTHIRM team's choices for the aircraft to be in the best possible locations given each day's conditions. For the latter two missions, the HYTHIRM team's decision to support the Edwards and not Kennedy reentries actually had to be rendered before the NASA's Shuttle Program made its decision. Once the observations were made, Mr. Osei-Wusu used both near real-time satellite data, as well as global climate models to estimate the radiative transfer effects along the atmospheric portions of the lines-of-sight. This was key to providing well-calibrated, well-corrected data for later processing efforts.

X. References

Periodicals

[1] Crow, D., Coker, C., and Keen, W., "Fast Line-of-sight Imagery for Target and Exhaust-plume Signatures (FLITES) scene generation program," Technologies for Synthetic Environments: Hardware-in-the-Loop Testing XI, edited by Robert Lee Murrer, Jr., Proc. Of SPIE Vol. 6208, 62080J, (2006).

[2] Berk, A., Anderson, G. P., Bernstein, L. S., Acharya, P. K., Dothe, H., Matthew, M. W., Adler-Golden, S. M., Chetwynd, Jr., J. H., Richtsmeier, S. C., Pukall, B., Allred, C. L., Jeong, L. S. and Hoke, M. L., "MODTRAN4 Radiative Transfer Modeling for Atmospheric Correction, SPIE Proceeding," Optical Spectroscopic Techniques and Instrumentation for Atmospheric and Space Research III, Volume 3756 (1999).

[3] Periaswamy, S., Farid, H.. "Elastic registration in the presence of intensity variations", IEEE Transactions on Medical Imaging, vol.22 no.7, July 2003.

Proceedings

[4] Anderson, B., Campbell, C., Kinder, J., Saucedo, L., "Boundary Layer Transition Flight Experiment Overview and In-Situ Measurements," AIAA-2010-240, January 2010.

[5] Tack, S., Tomek, D. M, Horvath, T. J., Verstynen, H. A., Shea, E. J., "Cast Glance Near Infrared Imaging Observations of the Space Shuttle During Hypersonic Re-entry," AIAA-2010-243, January 2010.

[6] Zalameda, J. N., Horvath, T. J., Tomek, D. M., Tietjen, A. B., Gibson, D. M., Taylor, J. C., Tack, S., Bush, B. C., Mercer, C. D., and Shea, E. J., "Application of a Near Infrared Imaging System for Thermographic Imaging of the Space Shuttle During Hypersonic Re-Entry," AIAA-2010-244, January 2010.

[7] Horvath, T. J., Tomek, D. M., Berger, K. T., Zalameda, J. N., Splinter, S. C., Krasa, P. W., Schwartz, R. j., Gibson, D. M., Tietjen, A. B., Tack, S., "The HYTHIRM Project: Flight Thermography of the Space Shuttle During Hypersonic Re-entry," AIAA-2010-241, January 2010.

[8] Wood, W. A., Kleb, W. L., Tang, C. Y., Palmer, G. E., Hyatt, A. J., Wise, A. J., McCloud, P. L., "Comparison of CFD Predictions with Shuttle Global Flight Thermal Imagery and Discrete Surface Measurements," AIAA-2010-454, January 2010.

[9] Caram, J. M., Bouslog, S. A., and Cunnington, G. R., Jr., "Emittance Measurements of Space Shuttle Orbiter Reinforced Carbon-Carbon," AIAA 93-0841, January 1993.

[10] Bouslog, S. A. and Cunnington, G. R., Jr., "Emittance Measurements of RCG Coated Shuttle Tiles," AIAA 92-0851, January 1992.

[11] Horvath, T., Berry, S., Splinter, S., Daryabeigi, K., Wood, W., Schwartz, R., and Ross, M., "Assessment and Mission Planning Capability For Quantitative Aerothermodynamic Flight Measurements Using Remote Imaging," AIAA 2008-4022, June 2008.

[12] Candler, G. V. and Campbell, C. H., "Hypersonic Navier-Stokes Comparisons to Orbiter Flight Data," AIAA-2010-455, January 2010.

[13] Tietjen,A., Wendt, J., Dawson, D., Ahlgreen, R., Blanchard, R., Welch, S., Lovern, M., "ISAFE Infrared Sensing Aeroheating Flight Experiment" AIAA-BMDO Tech Conf paper 7-9, July 2000.

Reports, Theses, and Individual Papers

[14] Space Program Operations Contract, Internal Interface Control Document: Ascent/Descent BET Product, ICD-I-TOP-003, Rev. D, United Space Alliance (USA) Contract NNJ06VA01C, January 22, 2007.

[15] Myers, T. M., McDonough, J., Noah, M., and Campbell, T., "PLEXUS (Phillips Laboratory Expert System-Assisted User Software)," Phillips Laboratory Technical Report PL-TR-97-2071, Hanscom AFB, MA, 1 March 1997.

[16] Periaswamy, S.. "General-purpose medical image registration", Ph.D. Dissertation, Department of Computer Science, Dartmouth College, 2003.

Computer Software

[17] AGI Satellite Toolkit (STK) http://www.stk.com/